J. Fluid Mech. (2005), *vol.* 524, *pp.* 131–142.
DOI: 10.1017/S0022112004001995 Printed in the United Kingdom

The transient behaviour of a large bubble in a vertical tube

By VOLKER BAUMBACH†, E. J. HOPFINGER AND A. CARTELLIER

LEGI, CNRS/INPG, Rue de la Piscine, B.P. 53, 38041, Grenoble, France

(Received 21 May 2004 and in revised form 5 August 2004)

Novel experimental results are presented of the transient motion of a large spherical-cap bubble and of the displaced liquid motion in a closed cylindrical vertical tube of finite length. This is a fundamental fluid mechanics problem and has direct application to Space flight where liquids in fuel tanks are exposed to large changes in acceleration. The initial spherical cap shape is produced by a thin membrane which can be considered equivalent to a large surface tension. The bubble is released by puncturing the membrane which, subsequently, retracts in a time of order 1 ms. Apart from the generation of shear instabilities of very short wavelength, the membrane withdrawal has a negligible effect on the bubble and liquid motions and can thus be considered instantaneous. The displacements of the bubble, the annular liquid sheet and the geyser front were determined from high-speed video images from which velocities and accelerations were calculated. The results are compared with a theoretical model of the unsteady bubble and sheet velocities.

1. Introduction

The steady-state behaviour of a large bubble rising in a vertical tube is well-known (Batchelor 1967). In a vertical circular tube which is closed at its top and open at its lower end, the steady-state rise velocity of the bubble is obtained from a local analysis of the flow around the cap of the bubble (Dimitrescu 1943; Davies & Taylor 1950). The observed bubble velocity, $U_b = 0.48\sqrt{gR}$, where g is the gravitational acceleration and R the tube radius, is close to the theoretical value determined from local analysis, neglecting viscous effects. The downward velocity of the annular sheet is given by free-fall conditions and is related, by mass continuity, to the bubble velocity via the sheet thickness d.

In most practical applications the main interest is in the rate at which the tube is emptied of its liquid when it is suddenly opened at its lower end. For long tubes knowledge of the steady-state behaviour is in this case adequate, because the distance to reach steady-state conditions is of the order of the tube diameter (Héraud 2002). However, there are situations where the tube is short and the transient behaviour must be taken into account. Naturally, this behaviour will depend on the initial conditions, that is on the shape of the initial interface. During Space flight for instance liquid propellants in fuel tanks are exposed to micro-gravity conditions and surface tension is then the dominant force which acts on the liquid. In this case, the shape of the liquid surface depends on the residual acceleration with respect to the surface tension force,

† Present address: Airbus Deutschland GmbH 28199 Bremen, Germany.

the ratio of which is expressed by the Bond number (see equation (3.7)). Depending on the residual perturbations, liquid can accumulate anywhere in the tank and often accumulates at the front of or at the top of the tank, i.e. opposite the fuel outlet. Before any restart of the engine it is necessary to position the liquid at the outlet at the bottom of the tank and this is done by applying a pre-acceleration. The situation we consider is that of a vertical closed circular container, partially filled with liquid which, in the initial state, is in the upper section of the container. The surface shape is nearly hemispherical and concave with respect to the vector normal to the liquid surface pointing toward the gas. This liquid is then suddenly exposed to a downward acceleration.

Experiments of this type, where a liquid, initially under micro-gravity conditions, is suddenly exposed to an acceleration, were conducted by Salzman & Masica (1968) and Salzman, Masica & Lacovic (1973) in a 145 m drop tower. These experiments focused on more global aspects of practical interest and, specifically, on the geyser which is formed when the liquid reaches the bottom of the container. Under terrestrial conditions such experiments have never been attempted, because the passage from a low to high Bond number state has to be accomplished in a very short time which raises considerable experimental difficulties.

It is shown in this paper that these difficulties can be overcome in the laboratory under terrestrial conditions by using membranes which simulate high surface tension. In particular, it is possible to maintain an initial state with the liquid at the top of the tank and with predefined curvature of the free liquid surface. In preliminary experiments we investigated different radii of curvature, ranging from infinity (horizontal membrane) to R, including convex shapes. When the membrane is horizontal, the classical Rayleigh–Taylor instability is observed. However, a slightly concave shape leads to bubble formation similar to that presented here. The time for the retreat of the membrane after its rupture is of order 1 ms, hence suddenly exposing a convex air cavity to gravity. Aside from its practical interest, this problem raises a number of fundamental questions, some of which will be considered in this paper. In § 2 the experimental set-up and procedures are described. A theoretical analysis of the bubble and liquid sheet motions is presented in § 3. The experimental results concerning the bubble shape and its dynamics as well as the liquid sheet dynamics, including geyser formation, are discussed in § 4.

2. Experimental set-up

The apparatus shown schematically in figure 1, consists of two cylindrical tubes of radius $R = 25\,\text{mm}$ closed at one end and of lengths L_1 and L_2 which can be varied independently from 5 to 70 mm. In the present experiment the tube lengths were $L_1 = 25\,\text{mm}$ and $L_2 = 56\,\text{mm}$. In figure 1, h_1 and h_2 refer to the initial liquid contact line which is either at the intersection of the two tubes or slightly above ($h_1 \geqslant L_1$ and $h_2 \leqslant L_2$). The lower tube is positioned with the open end upward and the upper one placed on top with the open end pointing downward. A stretched membrane is placed between the open ends of the tubes and the cylinders are then clamped together. Various membranes were tested and the final choice was a pure latex membrane of 7 μm in thickness. In preparing the experiments, an auxiliary frame was used to stretch the membrane evenly and always at the same rate. Once the membrane was in place, the liquid was introduced in the top tube separated by the membrane from the lower tube which contained gas (air for the present experiments). The liquid used was tap water with a surface tension $\sigma = 70\,\text{dyn}\,\text{cm}^{-1}$. Some experiments were

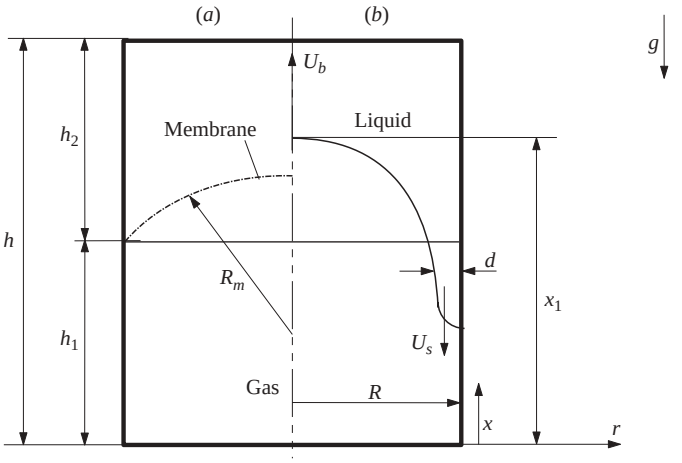

FIGURE 1. Experimental conditions and relevant dimensions of the cylindrical container of radius R: (*a*) initial conditions with the membrane in place; (*b*) conditions after rupture of the membrane indicating the rising bubble and the falling liquid sheet.

conducted with FC-77 of $\rho = 1.78\,\mathrm{g\,cm^{-3}}$, $\sigma = 15\,\mathrm{dyn\,cm^{-1}}$ and kinematic viscosity $\nu = 7.2 \times 10^{-3}\,\mathrm{cm^2\,s^{-1}}$ at 25 °C. The air pressure in the lower cylinder was then slightly increased to obtain the desired radius of curvature R_m of the membrane. In the present experiments $R_m \approx R$ and $h_1 = 28\,\mathrm{mm}$ is slightly larger than L_1. The liquid fill ratio could be varied by changing h_1 (L_1) with respect to h_2 (L_2). At time $t = 0$ the membrane was punctured in the middle by a thin pointed rod introduced from below. The retreat of the membrane occurred in about 1 ms. During this retreat a Kelvin–Helmholtz instability of very short wavelength was produced at the curved liquid surface which caused some local air entrainment and small bubble formation near the liquid surface. Because of its very short wavelength compared with the Rayleigh–Taylor instability wavelength or the cylinder radius, the Kelvin–Helmholz instability does not affect the liquid reorientation phenomena; it also decays relatively rapidly. For an experiment to be successful, a complete rupture of the membrane is absolutely necessary. After rupture, the remaining, very small, thin membrane pieces stuck to the wall and had practically no effect on the sheet motion. Moreover, there was also an annular gap of 1 mm in height and 3 mm depth between the two cylindrical tubes which allowed most of the membrane to withdraw completely. In some cases the membrane did not rupture completely and a segment remained attached. When this happened, the flow was asymmetric and it was easy to verify after each experiment whether or not complete rupture had occurred and eliminate experiments with incomplete rupture. Images were taken with a high-speed digital camera, Speed Cam Visariao 1500, at 500 frames per second. For the investigation of the initial retreat of the membrane, images at 10^4 frames per second were taken. For contrast improvement uniform backlighting was used. From these images the interface position and its shape as a function of time were determined by edge detection using a 3×3 sobel filter provided by Matlab^{TM}.

3. Theoretical analysis

When viscous effects can be neglected, a large gas bubble starting from rest in an unbounded liquid experiences an acceleration of $2g$, hence a velocity increase

$U(t) = 2gt$ (Batchelor 1967). In reality the velocity reaches a steady state because the bubble is subjected to a drag which is large when the bubble Reynolds number is large (Davies & Taylor 1950). The bubble shape changes during the acceleration phase and depending on the Bond number this change in shape may be non-monotonic giving rise to possible velocity oscillations. The present case is similar to this situation, except that the liquid is bounded and the bubble is actually a slug. Since the gas density $\rho_a \ll \rho$, ρ being the density of the liquid, the gas inertia can be neglected compared with the inertia of displaced liquid mass M_0. The equation of motion is then

$$k_a M_0 \dot{U}_b = g M_0 - D, \tag{3.1}$$

where k_a is the added mass coefficient, $M_0 = C_1 \rho \pi R^3$ and $D = \rho C_D \pi R^2 \frac{1}{2} U_b^2$, where C_D is the drag coefficient. The solution of equation (3.1) is

$$\frac{U_b}{U_{bs}} = \frac{e^{t/T} - 1}{e^{t/T} + 1}, \tag{3.2}$$

where the time constant $T = t_b \sqrt{C_1 k_a^2 / 2C_D}$ and the characteristic time scale $t_b = \sqrt{R/g}$. The ratio C_D/C_1, obtained from the steady-state velocity of a large bubble in a vertical cylindrical tube, $U_{bs} = 0.48\sqrt{gR}$, is $C_D/C_1 \approx 8.6$. The added mass coefficient is taken as $k_a = 0.5$ assuming a hemispherical shape. This value of k_a gives at $t = 0$, when $D = 0$, a bubble acceleration of $2g$. Note that the steady-state velocity is obtained from a local analysis of potential flow around the bubble cap (Davies & Taylor 1950; Batchelor 1967) and no drag is introduced. However, the bubble is subject to a drag, which needs to be introduced in the force balance, equation (3.1).

The front velocity of the descending annular liquid sheet U_{s1} (see figure 1 for definition) for $0 \leqslant x \leqslant h_1$ is given by free-fall conditions:

$$U_{s1} = -\sqrt{2g(h_1 - x)}. \tag{3.3}$$

The characteristic sheet time scale is then $t_s = \sqrt{h_1/g}$ and the velocity scale is $U_1 = \sqrt{2gh_1}$. After the front of the sheet has reached the bottom, the sheet velocity will change to

$$U_s = -\sqrt{2g(x_1 - x)}, \tag{3.4}$$

where $x_1(t)$ is the distance from the bottom to the nose of the bubble (see figure 1). The maximum sheet velocity is obtained at $x = 0$ when $x_1 = h$, which corresponds to the total tube height. In the steady state the relation between U_s and U_b is given by mass conservation and is

$$U_s \approx \frac{0.48\sqrt{gR}}{1 - (R - d/R)^2}, \tag{3.5}$$

where d is the sheet thickness at position x and is of order $d/R \approx 0.17\sqrt{R/(x_1 - x)}$ (Batchelor 1967). In equation (3.5) it was assumed that $(d/R)^2 \ll 1$ which is the case. Surface tension does not affect the bubble nor the sheet velocity (except for the incipient sheet motion and possible front speed oscillations, see § 4.3). It has a stabilizing effect on possible perturbations of the bubble cap and determines the wavelength of a possible instability of the front of the falling liquid sheet. The geyser front which emerges when the liquid converges at the centre of the bottom plate is also affected by surface tension. The characteristic parameter is the Weber number

$$We = \frac{\rho U^2 R}{\sigma}, \tag{3.6}$$

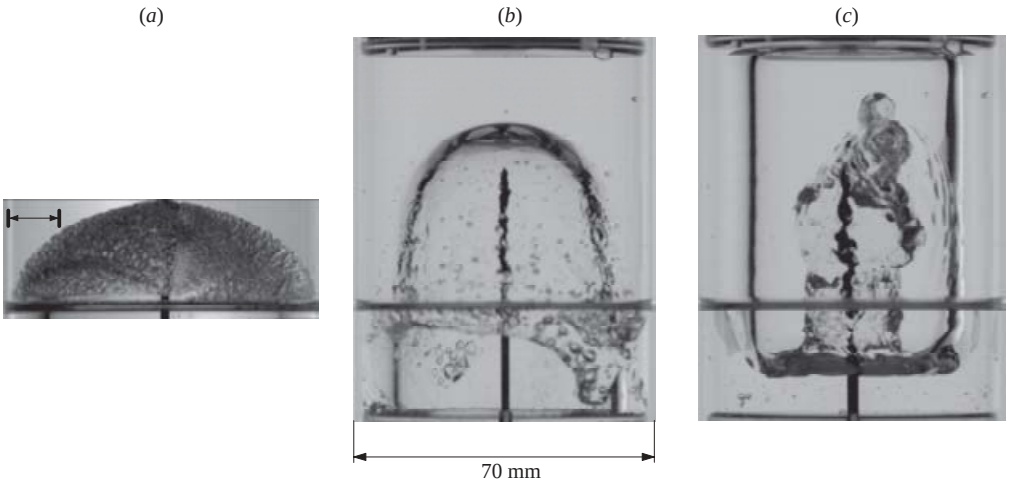

FIGURE 2. Images of the flow development: (*a*) a focus on the Kelvin–Helmholtz instability at $t = 1.2$ ms after membrane rupture, caused by the withdrawal of the membrane; (*b*) front of the downward moving liquid sheet at $t = 68$ ms; (*c*) geyser at $t = 184$ ms. The experimental conditions are: $R = 25$ mm, $h_1 = 28$ mm, $h_2 = 56$ mm, $R_m = 23.4$ mm. The liquid is tap water at 22 °C.

where U is the velocity either of the bubble U_b or of the falling sheet or of the rising geyser. The corresponding characteristic Bond numbers are obtained by simply substituting the respective expressions for U. A characteristic liquid reorientation Bond number is therefore

$$Bo = \frac{\rho g R h}{\sigma} \tag{3.7}$$

and the characteristic Bond number of the bubble, which gives an indication of the stability of the bubble cap, is

$$Bo_b = \frac{\rho g R^2}{\sigma}. \tag{3.8}$$

Viscous effects with respect to surface tension forces, expressed by the Ohnesorge number, $Oh = \rho \nu^2 / \sigma R < 10^{-3}$, can be ignored, where ν is the kinematic viscosity.

4. Experimental results

4.1. *Qualitative observations*

The evolution of the flow is shown in figure 2, starting with the rupture of the membrane at $t = 0$ (figure 2*a*) up to geyser formation (figure 2*c*). The reorientation Bond number in these experiments is $Bo = 300$ and $Bo_b = 89$. The time of withdrawal of the membrane is $t_m \approx 1.1$ ms which is two orders of magnitudes less than the characteristic bubble time scale of $t_b = \sqrt{R/g}$. The mean velocity of membrane withdrawal U_m is of order $0.5\pi R_m / t_m \approx 35\,\mathrm{m\,s^{-1}}$ and the thickness of the shear layer, produced at the liquid surface by this withdrawal, varies from practically zero at the centre to $\delta \sim 7\sqrt{\nu t_m} \sim 0.2$ mm near the tube wall. The corresponding Reynolds number is $Re = U_m \delta / \nu \leqslant 7 \times 10^3$. Thus, a Kelvin–Helmholtz instability of wavelength λ_{KH} can be expected. The observed spacing of the Kelvin–Helmholtz billows near the tube wall (see figure 2*a*) agrees with the estimated wavelength. These small-scale perturbations have no effect on the initial flow development because any other length

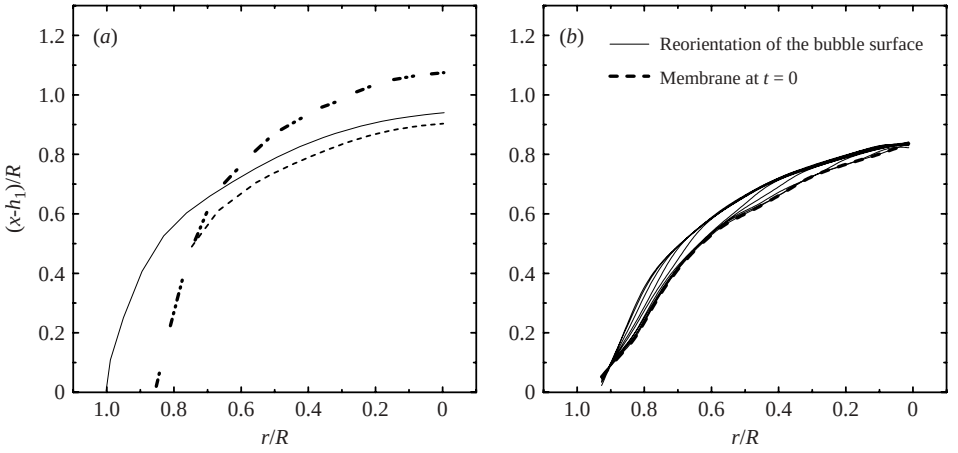

FIGURE 3. (*a*) Evolution of the bubble shape: dashed line $t = 0$ (start of the membrane rupture); solid line $t = 2$ ms; dash dotted line $t = 20$ ms. (*b*) Evolution of the outer edge during the first 1 ms at time intervals of 0.1 ms. The lower, dashed line corresponds to the membrane shape at $t = 0$. Note that (*a*) and (*b*) correspond to two different experiments which is the reason why the maxima of the membrane are slightly different.

scale is two orders of magnitude larger than λ_{KH}. Besides, these billows decay in a time of about $5t_m$. The main effects of this instability are the entrainment of a small gas volume, creating small bubbles (seen in figure 2*b*), and a small initial change (of the order of λ_{KH} after rupture) of the apparent bubble contour which is variable with radius R.

Figure 2(*b*) indicates the development of an instability of azimuthal wavelength of order πR (in the case of water) for the front of the falling liquid sheet. Under free-fall conditions, surface tension should prevent the development of an instability. This instability is likely to arise from the initial acceleration of the liquid sheet. On the other hand, the bubble cap is seen to remain stable. The Weber number from equation (3.6) is about 20 if calculated with R. If it is expressed in terms of the cap radius after bubble adjustment, it falls to less than about 7 (the radius of curvature of the bubble is about $0.6R$). Stability of the bubble cap is, therefore, to be expected. In experiments with FC-77 the bubble cap is less smooth but the mean motion of the bubble is not different from that of water (the density does not enter the bubble motion). The geyser, shown in figure 2(*c*) is almost at its maximum height and is exposed to a deceleration of $-g$ which means that the geyser front is in a nearly weightless state. Surface tension then controls the size of the surface corrugations and the size of a precursor geyser.

4.2. *Evolution of the bubble shape*

4.2.1. *Bubble shape*

From high-speed video images, recorded at a frequency of 500 frames per second, the time evolution of the bubble shape was determined by the above-mentioned edge detection method. The evolution of the bubble shape, obtained after optical corrections in the radial and axial directions, is shown in figure 3(*a*) for $t = 2$ ms and $t = 20$ ms. The dashed line corresponds to the membrane shape. It is seen from figure 3(*a*) that for longer times the radius of curvature decreases and the sheet thickness increased at $x = h_1$ increases. The time $t = 20$ ms corresponds closely to the adjustment time t_a of the bubble shape. For water this time is of the same order as

the sheet motion delay time t_d when the sheets leading edge starts to move downward. For FC-77 the delay time is considerably shorter (see § 4.3).

In figure 3(*a*), the first large change in interface position during a time interval of 2 ms from the membrane shape (dashed line) to the free liquid surface (solid line) is partly an apparent change due to the growth of the Kelvin–Helmholtz instability. This change is shown in figure 3(*b*) during the first 1 ms, where it is seen that the change in the outer edge increases with radius and decreases to zero close to the wall where the membrane velocity is again zero. The interface is shown at 0.1 ms intervals by the solid lines, going from the centre toward the wall, between the dashed curve and the outer solid line, which corresponds to the interface at 1 ms after rupture. Toward the tube wall the optical correction of the visible outer edge, shown in figure 3(*b*), is incomplete because the optical properties of the membrane there were poor and so ignored. For this reason, the interface does not end at $r/R = 1$ as it should. In order to avoid confusion we show, therefore, in figure 3(*a*) the outer edge when the membrane is in place (dashed line) only up to $r/R \approx 0.8$. Even for larger times the optical correction near the wall remains somewhat uncertain. It is seen in figure 3(*a*) that at time $t = 20$ ms the sheet thickness at $x \approx h_1$ is about $0.15R$.

4.2.2. *Bubble velocity*

For the determination of the bubble velocity and its acceleration, a mean value of the displacement of the bubble edge between $0 < r/R < 0.20$ was used. This acts as a filter which is applied because the bubble shape is not completely smooth and space and time intervals are very small; it is well-known that small errors in displacement cause large changes in acceleration. The displacement of the central part of the bubble, the calculated velocities and the accelerations are shown in figure 4 as a function of the dimensionless time t/t_b.

In figure 4(*a*) the measured bubble displacement corresponds to the open symbols. The dashed line indicates a slightly smoother displacement provided by a cubic spline fit. For comparison the theoretical displacement, obtained from integration of equation (3.2), is shown by the solid line. The agreement can be considered as excellent up to $t/t_b \approx 2.5$ except near the origin where the predicted displacement is slightly less than the observed one. For $t/t_b > 2.5$ the bubble is influenced by the upper end of the tube and starts to slow down. The bubble velocity given in figure 4(*b*), non-dimensionalized by the steady-state velocity, was obtained by a five-point differentiation of the cubic spline fitted curve. It can be seen that the initial velocity increase is more rapid than predicted by equation (3.2) but then falls slightly below the theoretical predictions until it increases to the steady-state velocity at $t \approx t_b$. However, small oscillations in velocity around the steady state value persist.

The corresponding acceleration shows larger fluctuations because the second time derivative of the bubble displacement amplifies the oscillations as well as small errors in the displacement at time increments of 0.002 s. Figure 4(*c*) shows, nevertheless, that the initial acceleration is at least $2g$. It is not possible to give a definite value for the initial acceleration but the initial velocity increase (see figure 4*b*) suggests that the acceleration is somewhat larger than the theoretical value $2g$. This would mean that the added mass coefficient is less than 0.5, which is plausible because of the change in bubble shape and the presence of the wall which limits the liquid motion. After the maximum, the acceleration drops rapidly to zero and even to negative values, probably because the displaced liquid is influenced by the tube sidewall and the bubble shape must change. Then, the acceleration fluctuates around zero in accordance with the velocity fluctuations. The difference between the observed bubble dynamics and

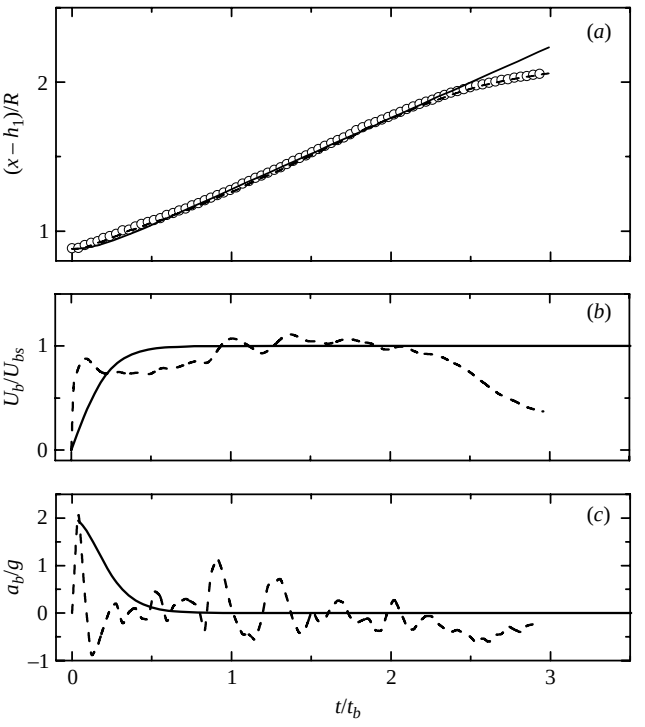

FIGURE 4. Dynamics of the rising bubble. (*a*) Bubble displacement as a function of dimensionless time t/t_b. The symbols are measured values and the dashed line is a cubic spline fit. (*b*) Calculated bubble velocity and (*c*) bubble acceleration (dashed lines). The solid lines in (*a–c*) are the theoretical variations given by equation (3.2) which is integrated for displacement and differentiated to obtain accelerations. The reference velocity is $U_{bs} = 0.48\sqrt{Rg} = 23.9\,\mathrm{cm\,s^{-1}}$ and the time scale is $t_b = \sqrt{R/g} = 50\,\mathrm{ms}$. The liquid is water but results are the same for other liquids.

that predicted by the model during the adjustment phase is to be expected because the theoretical model assumes constant bubble shape, constant drag and constant added mass coefficient which is certainly an oversimplification. The comparison is nevertheless useful and interesting.

In § 4.2.1 we mentioned that the bubble shape adjusts in a time t_a to the steady-state shape. Figure 5 shows that the bubble oscillates around the steady-state shape but the adjustment is nearly completed at $t_a \approx 0.4t_b$ when the acceleration is close to zero. This gives $t_a \approx 20\,\mathrm{ms}$.

4.3. *Falling sheet velocity*

The displacement of the descending liquid sheet was determined from a manual edge detection of the front between the two noses (see figure 2*b*). The velocity and acceleration were also determined from a numerical five-point differentiation of the cubic spline fit to the measured displacement. The results are shown in figure 5 for the same experimental conditions as in figure 4 as well as for FC-77. Here, the velocity, shown in figure 5(*b*), is non-dimensionalized by $U_1 = \sqrt{2gh_1}$ and the time by $t_s = \sqrt{h_1/g}$. What can be clearly seen in figures 5(*b*) and 5(*c*) is that the onset of the liquid sheet motion is delayed by a time $t_d/t_s \approx 0.38$ when the liquid is water and by $t_d/t_s = 0.16$ when the liquid is FC-77. This time delay t_d was determined by fitting the integrated form of equation (3.3), which is $x/h_1 = 1 - 0.5((t - t_d)/t_s)^2$

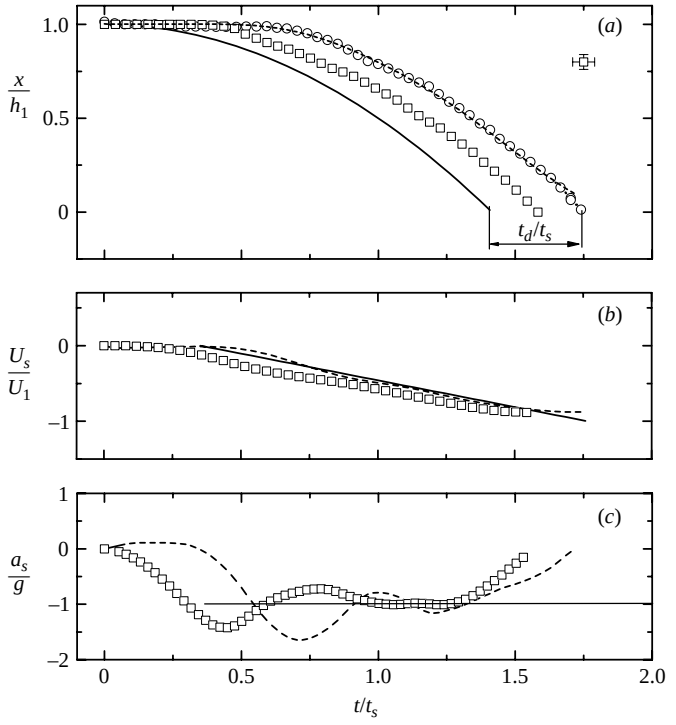

FIGURE 5. Dynamics of the falling sheet. (*a*) Displacement; the open circles represents water and the open squares represents FC-77; the dashed line represents a cubic spline fit for the displacement of water, where the solid line leaves the theoretical displacement according to $x/h_1 = 1 - 0.5(t/t_s)^2$; (*b*) the corresponding non-dimensional velocity versus time; (*c*) the corresponding non-dimensional acceleration. $U_1 = \sqrt{2gh_1} = 75.1\,\mathrm{cm\,s^{-1}}$, $t_s = \sqrt{h_1/g} = 53\,\mathrm{ms}$. In (*b*) the solid line is shifted by t_d (for water) to show the (small) oscillations of the velocity for the entire free fall. These oscillations are amplified when the acceleration is considered in (*c*).

to the experimental points. Then, the sheet accelerates rapidly and even exceeds g, after which it returns and oscillates around g (probably related to capillarity). When the liquid sheet is in free fall conditions, a fluid element within the liquid sheet is in a weightless state due to inertia and the compensation of the body forces. The instability of the sheet front which develops into the noses (figure 2*b*) must, therefore, be initiated near the origin when the sheet starts to accelerate. During the free fall the noses no longer grow.

Now coming back to the time delay, this is most likely caused by surface tension and possibly contact angle effects. After membrane withdrawal, the Bond number of the sheet $Bo_s = \rho g d^2/\sigma$ is small and at the sheet leading edge surface tension forces initially dominate over gravitational forces. We can assume that the sheet starts to move when $Bo_s \sim 1$. This gives a thickness of the sheet's leading edge $d_c \sim \sqrt{\sigma/\rho g}$ which is the capillary length. The time needed to reach this thickness, which is referred to as the incipient sheet motion delay time t_d, is directly related to the bubble motion: $t_d \sim d_c/U_b \sim \sqrt{\sigma/2\rho g R}$. Since U_b is independent of liquid properties, t_d depends only on $\sqrt{\sigma/\rho}$ for fixed g and R. The measured ratio of $t_{d_{water}}/t_{d_{FC-77}}$ is 2.8 and the corresponding ratio of $\sqrt{\sigma/\rho}$ is 2.9. The ratio $t_d/t_b \sim d_c/R$ and experiments give $t_d/t_b \approx 4d_c/R$ and $t_d/t_a \approx 10d_c/R$. Viscous effects on the sheet motion remain negligible because the sheet Reynolds number $Re_s = U_s d/\nu$ is of order 10^3.

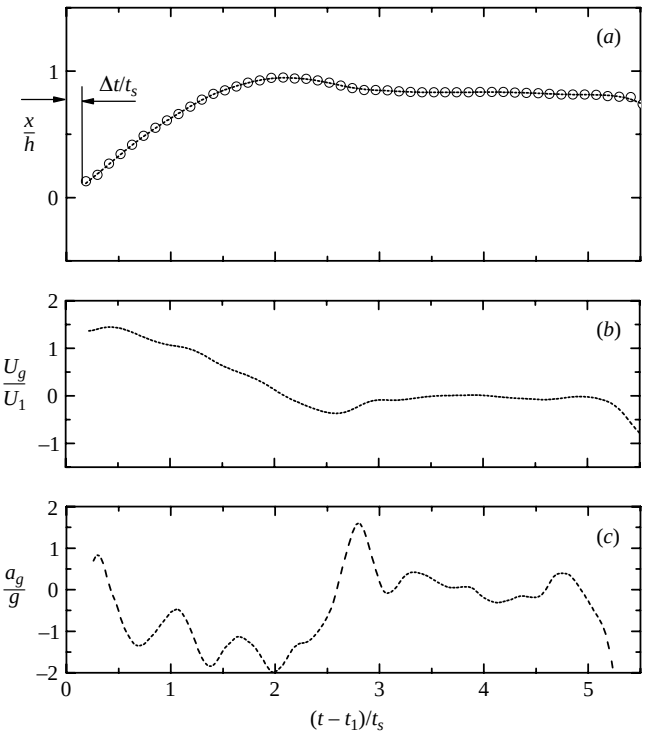

FIGURE 6. Geyser tip dynamics: (*a*) displacement, (*b*) velocity, and (*c*) acceleration, as a function of non-dimensional time $(t-t_1)/t_s$, where t_1 is the time when the sheet front arrives at the bottom. Position and velocity are non-dimensionalized with the height h and characteristic sheet front velocity $U_1=\sqrt{2gh_1}$ respectively. The time Δt refers to the delay between sheet impact and geyser emergence, which depends on the tube radius.

It is seen from figure 5(*c*) that as the sheet approaches the bottom plate the acceleration decreases and the non-dimensional velocity does not quite reach -1 (see figure 5*b*) as it should ideally. As the bottom is approached the noses arrive first and start to turn inward and this seems to affect the velocity of the whole sheet. Furthermore, if the sheet were to accelerate uniformly with g from $x=h_1$ to $x=0$, shown in figure 5 by the solid lines, the time needed to reach the bottom would be $t_1=\sqrt{2h_1/g}$ according to equation (3.3). The experimental results show that the actual time is larger due to the time lag related to surface tension effects as discussed above. In figure 4(*b*) it is seen that for water this time is close to the time needed for the bubble to adjust to the steady-state shape but is considerably smaller for FC-77.

4.4. *The rising geyser*

After the sheet has reached the bottom and the liquid merges at the centre, a geyser develops. In figure 6 the geyser tip position (*a*), its velocity (*b*) and its acceleration (*c*) are plotted as a function of non-dimensional time $(t-t_1)/t_s$, where t_1 is the time of arrival of the sheet front at the bottom which is different for water and FC-77 because t_d is different. From figure 6 it is seen that the geyser emerges when $(t-t_1)=\Delta t$ with Δt being of order $R/\sqrt{2gh_1}$. The experimental value is $\Delta t\approx 0.3R/\sqrt{2gh_1}$.

In figure 6 the position is non-dimensionalized by the total tube height h and the velocity by $U_1=\sqrt{2gh_1}$ which allows a comparison of the geyser velocity with the maximum sheet front velocity. Note that the geyser velocity is initially larger than

the maximum free-fall sheet front velocity. According to equation (3.4), the sheet velocity at $x = 0$ has to increase from $\sqrt{2gh_1}$ to $\sqrt{2gx_1}$ after the sheet front has arrived at the bottom. Using conservation of momentum and flow rate, it is easily shown that the geyser velocity near the bottom is initially equal to the sheet velocity at $x = 0$. Accordingly, the geyser diameter near the bottom is $R_g \approx \sqrt{2Rd} \approx 0.5R$. Figure 6(*b*) shows that the geyser front velocity initially increases and then decreases with time and goes to zero when the geyser is near its maximum height. There is, actually, a slight overshoot in height (see figure 6*a*) followed by a small negative velocity. Then, the geyser height remains nearly constant up to about $(t - t_1)/t_s \approx 5$ and collapses thereafter when the liquid in the sheet is nearly fully drained. The acceleration reaches initially about g and then decreases to less than $-g$ before it increases again. This irregular behaviour is caused by the nose of the geyser (see figure 2*c*) which changes in shape with small protrusions appearing and disappearing in a quasi-periodic manner.

5. Conclusion

The investigation of the transient behaviour of a large bubble in a vertical cylindrical tube and of the related motion of the liquid sheet has been made possible by a novel technique developed for creating a clean initial state. This technique consists of the use of a stretched thin membrane which, when punctured, retreats in a time negligible compared with the characteristic times of bubble adjustment or liquid motion. The remaining small membrane fragments have no effect on the liquid motion. The initial curvature of the membrane can be varied at will to simulate any desired initial Bond number. Previous studies of liquid reorientation were performed under micro-gravity conditions in a drop tower which has the drawback that observation times are very short and experiments are very costly and cumbersome. The results presented here, which show the time evolutions of the bubble and the sheet and geyser velocities, are novel. In particular it is shown that the bubble and sheet accelerations exceed initially the Earth's gravity g. For the rising bubble this is expected from the theoretical model proposed but for the falling sheet front it is unexpected. The initial geyser velocity is shown to be larger than the sheet front impact velocity at $x = 0$ which is consistent with the change in relevant length scale from h_1 before sheet impact to x_1 after impact. The theoretical model developed for the transient motion of the bubble and the liquid sheet contains the relevant physics and provides a useful comparison for the experimental results.

This work was initiated and financed by the COMPERE program through contract CNES n° 04/CNES/1616. We wish to thank one of the referees for drawing our attention to possible surface tension effects on the incipient motion of the liquid sheet. Special thanks go to François Bonnel for making the high-speed video imaging possible.

REFERENCES

Batchelor, G. K. 1967 *An Introduction to Fluid Dynamics*. Cambridge University Press.

Davies, R. M. & Taylor, G. I. 1950 The mechanics of large bubbles rising through extended liquids and through liquids in tubes. *Proc. R. Soc. Lond.* A **200**, 237–390.

Dimitrescu, D. 1943 Strömung an einer Luftblase im senkrechten Rohr. *Z. Angew. Math. Mech.* **23**, 139–149.

Héraud, P. 2002 Etude de la dynamique des bulles infinies: application à l'étude de la vidange et du remplissage de réservoirs. Thèse de Doctorat, Université de Provence Aix-Marseille.

Salzman, J. A. & Masica, W. J. 1968 Experimental investigation of liquid-propellant reorientation. *NASA TN* D-3789; also in *Low Gravity Propellant Orientation and Expulsion*. AIAA Lecture Notes, vol. 6 (ed. W. Heller).

Salzman, J. A., Masica, W. J. & Lacovic, R. F. 1973 Low-gravity reorientation in a scale-model Centaur liquid-hydrogen tank. *NASA TN* D-7168.